

S4: A Spatial-Spectral model for Speckle Suppression

Rob Fergus^{1,2}, David W. Hogg³, Rebecca Oppenheimer⁴, Douglas Brenner⁴,
 Laurent Pueyo^{5,6}

ABSTRACT

High dynamic-range imagers aim to block out or null light from a very bright primary star to make it possible to detect and measure far fainter companions; in real systems a small fraction of the primary light is scattered, diffracted, and unocculted. We introduce *S4*, a flexible data-driven model for the unocculted (and highly speckled) light in the *P1640* spectroscopic coronograph. The model uses Principal Components Analysis (PCA) to capture the spatial structure and wavelength dependence of the speckles but not the signal produced by any companion. Consequently, the residual typically includes the companion signal. The companion can thus be found by filtering this error signal with a fixed companion model. The approach is sensitive to companions that are of order a percent of the brightness of the speckles, or up to 10^{-7} times the brightness of the primary star. This outperforms existing methods by a factor of 2-3 and is close to the shot-noise physical limit.

1. Introduction

High dynamic range imaging and spectroscopy is the next frontier in the study of exoplanets (Oppenheimer & Hinkley (2009); Oppenheimer et al. (2012); Traub & Oppenheimer (2010)). There is hope for atmospheric spectroscopy of substantial numbers of giant planets, direct detection of planets at large albedo and radius, and eventually—with something like the far-future *Terrestrial Planet Finder*—direct time-domain imaging and spectroscopy of

¹Department of Computer Science, New York University

²to whom correspondence should be addressed: fergus@cs.nyu.edu

³Center for Cosmology and Particle Physics, Department of Physics, New York University

⁴Department of Astrophysics, American Museum of Natural History

⁵Space Telescope Science Institute, Baltimore

⁶Dept. of Physics and Astronomy, Johns Hopkins University

Earth-like planets around other stars. All of these projects involve exceedingly precise optical designs, in which the light from the (generally bright) primary star is more-or-less nulled, at least for certain locations on the focal plane. Starlight suppression is achieved using diffraction and carefully designed optics that remove starlight. However, this can never be accomplished perfectly because residual scattered light due to optical path length differences within the beam cannot be controlled using diffractive techniques. For example, simply detecting an earth analog around a star 10 pc away requires wavefront control on the level of $\lambda/10000$. Obtaining a spectrum through the optical and IR would require wavefront control at the level of $10^{-5}\lambda$, or roughly 10 picometers. However, projects are making advances in this direction, with some beginning to demonstrate nanometer level optical control on real telescopes. In any case, these projects and the more ambitious ones planned for the future require very sophisticated instrument models and software pipelines that implement them to achieve full sensitivity.

A working example is the *P1640* spectroscopic coronograph. Project 1640 recently demonstrated 5 nm on-sky control of starlight for observations in the range $\lambda = 0.98\text{--}1.75\mu\text{m}$ (Oppenheimer et al. (2012)). This project, the first of several similar instruments, involves the world’s highest order adaptive optics system (Dekany et al. (2006); Roberts et al. (2012)), an optimized apodized pupil Lyot coronagraph (Soummer (2005)), an integral field spectrograph (Hinkley et al. (2011)), and a calibration interferometer to detect remnant wave front errors at the starlight suppression optics (Wallace et al. (2010); Zhai et al. (2012)). The project has pioneered many aspects of this complex suite of instrumentation including data reduction techniques (Zimmerman et al. (2011)) and rapid faint companion characterization (Zimmerman et al. (2010)). In addition, the project has explored post-processing techniques to improve sensitivity (Crepp et al. (2011); Pueyo et al. (2011)). The images produced by *P1640* have the vast majority of the light from the primary star nulled at the focal plane. The remaining light falls in a highly speckled pattern produced by constructive and destructive interference of residual imperfections in the wavefronts entering the instrument, made worse by differential chromatic aberration. The speckle pattern is quasi-random but has some overall variation with wavelength, somewhat like the pure angular expansion with wavelength that would be expected for perfect optics, but not exactly (Bloemhof et al. (2001); Racine et al. (1999); Hinkley et al. (2007)). See Fig. 1 for two example cubes of FU ORI at 3 different wavelength bands.

In principle, a wavelength-level model of the wavefronts and all optical (and non-optical) surfaces in the *P1640* system would produce a precise model of the intensity maps read out at the detector. Naively, this model would have of order 10^{12} parameters and be intractable to instantiate, let alone fit or optimize. Without this model, the speckles are stochastic but with strong regularities. This suggests data-driven modeling, or using the *data that the*

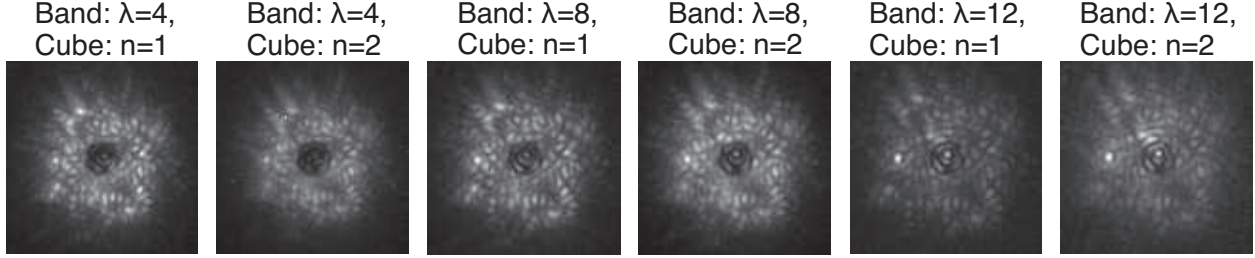


Fig. 1.— Examples of 3 different wavelength bands from 2 different cubes from the star FU Ori. Note the subtle variation between the different cubes, due to changes in atmospheric PSF, as passed through the coronagraph optical train.

instrument has in fact taken to build a precise and informative but flexible model of the data that it *can* produce. If this model can be trained on data that do not have—or are not expected to have—faint companions contributing, then companions can be detected as failures of the model, or successes of a model that is a superposition of the data-driven model and a model companion.

Of course, we do not know in advance which stars will have companions; we do not have tagged data for training what are known as “supervised” methods. Relying on the fact that detectable companions are rare, we adopt a “train and test” framework, in which we use, when looking for a companion at a particular location in the focal plane, all the data in the data set *not* at that location to train the model. At the same time, we have very severe precision requirements, because we are looking for companions that are far fainter than the residual intensity in the instrument. This latter requirement pushes us towards models for the unblocked light that are extremely flexible, but not so flexible that they can absorb light from companions. We will end up getting good performance by using models with dozens to hundreds of parameters in every small patch of the focal plane.

In this Article, we present a new methodology—*S4*—for modeling high dynamic-range data that is extremely effective when the images are spectroscopically sliced. The basic principle is to build a model that jointly captures the spatial and spectral structure of the data. This is needed to build an effective model of the speckles since their spatial pattern evolves in a distinctive and predictable way as a function of wavelength. While a range of models are possible, we adopt Principal Components Analysis (PCA), also known as the Karhunen-Loeve transform. This assumes the data lies on a linear subspace of low dimensionality, compared to the input dimension. This is a valid assumption for our data as the speckles have distinctive structure to them, being far from I.I.D. random noise, hence much of the energy of the signal can be captured by a linear subspace of a few hundred dimensions at most, far lower than the number of pixels in the cubes (see Fig. 4(right)).

Another advantage, given the limited number of exposures of a given star, is that PCA requires relatively little data to build a model. More complex models such as sparse coding (Tibshirani (1996); Mairal et al. (2009)) could also be used, but requires more data than is typically available in our application. The full S_4 algorithm enables both the detection and spectral analysis of exoplanets, but this *Article* only address the detection problem. A forthcoming paper will explain its use for spectral extraction.

S_4 benefits from an interdisciplinary collaboration bringing together astronomy and computer vision. We demonstrate the method with *P1640* data, and release working code.

1.1. Related Work

Several other techniques for speckle suppression have recently been proposed. LOCI Lafreniere et al. (2007) and variants Pueyo et al. (2011) attempt to fit the speckles using a linear combination of patches from nearby wavelengths/exposures. As noted by several authors (e.g. Marois et al. (2010)), this approach risks the possibility of companion flux being accidentally being removed which impairs performance. Correspondingly, a number of refinements have been proposed, most notably the SOSIE pipeline Marois et al. (2010). A notable difference to S_4 is that these approaches rely on the use of Angular Difference Imaging (ADI), which we do not use (since the telescope on which the *P1640* instrument is mounted has an equatorial mount). In our experiments, we also make a direct comparison to the damped LOCI algorithm of Pueyo et al. (2011).

Two recent papers also use PCA to model the speckle pattern. *KLIP* by Soummer et al. (2012) has some close similarities to S_4 in that it uses principal components of the observed data variance to build a reduced-dimensionality description of the data, which is used in turn as a model. The principal differences between *KLIP* and S_4 arise from the fact that *KLIP* is designed to work on *Hubble Space Telescope* data, which, though variable, do not show as much variation as ground-based data. Furthermore, the *HST NICMOS* images are not dispersed, so there is no way to use expected or approximate variations of speckle patterns with wavelength. Correspondingly, *KLIP* uses PCA to capture the spatial structure of the speckles, differing from S_4 that models the joint *spatial-spectral* structure. As spectral dispersion provides valuable information about the speckle morphology in each wavelength slice, S_4 is better suited to capturing this structure.

Amara & Quanz (2012) also propose a PCA based model. In contrast to S_4 which models local image patches with PCA, this work attempts to model the whole speckle field in with a single PCA basis. Using local model patches has the advantage that the speckle

structure can be captured with far fewer components than a global model. This work also relies on the using of ADI.

2. Method

While we describe our approach in the context of the *P1640* instrument, the algorithm does not rely on any special properties of the device, thus can potentially be applied to data produced by other coronagraphs of the same type. We do not take advantage of techniques such as Angular Difference Imaging (ADI), but these could potentially be combined with our approach to improve performance.

We assume as input to the algorithm properly calibrated intensity information $I_{x,y,\lambda,n}$ on a four-dimensional boxel grid where the (x, y) indices indicate a pixel number on a regular square pixel grid in the focal plane, the λ index indicates one of a set of narrow wavelength bins, and the n index is exposure or “cube” index in the multiple exposures that make up the data set for any one star. $I_{x,y,\lambda,n}$ has dimensions $[X \times Y \times \Lambda \times N]$. For the *P1640* data used in our experiments, $X = Y = 101$, $\Lambda = 32$ and $N \sim 10$, depending on the star.

In brief, we are going to build a model for each patch in this data by taking representative sets of patches (training sets) and building a PCA-based data-driven model for it. The model is then subtracted from the patch and the residual compared to test PSF’s. In the following explanation we use images of the star FU Ori as a running example; it has a bright companion embedded in speckle artifacts that allows easy confirmation of the method’s efficacy. A summary of the approach is given in Algorithm 1.

2.1. Pre-processing

The main pre-processing step is the spatial alignment of the data to ensure that the star is centered within $I_{x,y,\lambda,n}$. Due to atmospheric dispersion at off-zenith viewing angles, the location of the star varies with wavelength, thus centering must be performed for each wavelength λ , as well as each cube n . Currently this is performed semi-automatically, using the four control spots in the *P1640* data created by diffraction off of a grid of thin wires in the instrument. The spots are manually identified by a user for each λ, n slice of $I_{x,y,\lambda,n}$. The local maxima around each user click is found and the centroid of the four maxima computed, which gives the position of the star. Each slice is then translated (with sub-pixel accuracy) so that the star is centered.

2.2. Polar transform

For PCA to be an appropriate model choice, the data must lie on a linear subspace of low-dimensionality. Correspondingly, we make use of an important property of the data $I_{xy\lambda n}$, namely that the evolution of the speckles with wavelength is mostly radial (see Figure 3(bottom) for validation of this). In the original cartesian representation this radial structure is distinctly non-linear, thus hard to model with PCA.

We therefore apply PCA to a polar transformation of the data, instead of in the original cartesian space. In the polar space, the structure of the speckles is well captured by a joint 2D model of radius and λ , since their tangential motion is small. By contrast, in the cartesian space, a joint 3D model over x, y, λ would be needed.

More precisely, we take centered annular sections of $I_{xy\lambda n}$, at radius d , having width R and transform each (λ, n) plane separately to a polar representation using bicubic interpolation, with application of the appropriate Jacobian. The number of samples Θ in orientation is $\lceil 2\pi d \rceil$, chosen to ensure the signal is well-sampled. This results in a 4D polar data array $J_{r,\theta,\lambda,n}$ of dimension $[R \times \Theta \times \Lambda \times N]$, where $R \sim 20 - 30$ typically. Fig. 2 shows an example of the input data $I_{x,y,\lambda,n}$ in cartesian representation, along with the polar projection $J_{r,\theta,\lambda,n}$ of an annular band, both averaged over λ and n . Fig. 3 shows different visualizations of $J_{r,\theta,\lambda,n}$ which reveal the structure of the speckles.

2.3. PCA Patch Model

Examining Fig. 3(bottom), we see that speckle structure extends over a small angular range, rather than being confined to a single angle. Thus, to capture the speckle structure, we apply PCA to *patches* extracted from $J_{r,\theta,\lambda,n}$ that have a narrow window over angle $\theta \pm (\Phi/2)$ and full extent over radius r and wavelength λ . For a given angle θ and cube n , each patch $P_{r,\phi,\lambda}^{\theta,n}$ is a 3D volume of dimension $[R \times \Phi \times \Lambda]$, where the extent over angle Φ is small, typically $\sim 3 - 5$ pix, chosen to (i) reflect the characteristic diffraction scale and (ii) to keep the patch dimensionality to a reasonable level. Patches are extracted from $J_{r,\theta,\lambda,n}$ in “sliding window” fashion, i.e. at every θ location, with circular boundary conditions. $J_{r,\theta,\lambda,n}$ is thus expanded into a set of $\Theta \cdot N$ patches $P_{r,\phi,\lambda}$, each of dimension $[R \times \Phi \times \Lambda]$.

At a given radius d , we systematically test each angle θ for the presence of a companion. This is done by splitting the patches into disjoint *training* and *test* sets. The training set will be used to construct a linear speckle model, based on a PCA eigenvector basis, while the test set will be fit with those eigenvectors to leave a residual that potentially may contain a companion. The test set P_{test} is the union of patches close in angle to θ : $P_{test} = \{P^{\theta,n}\}$

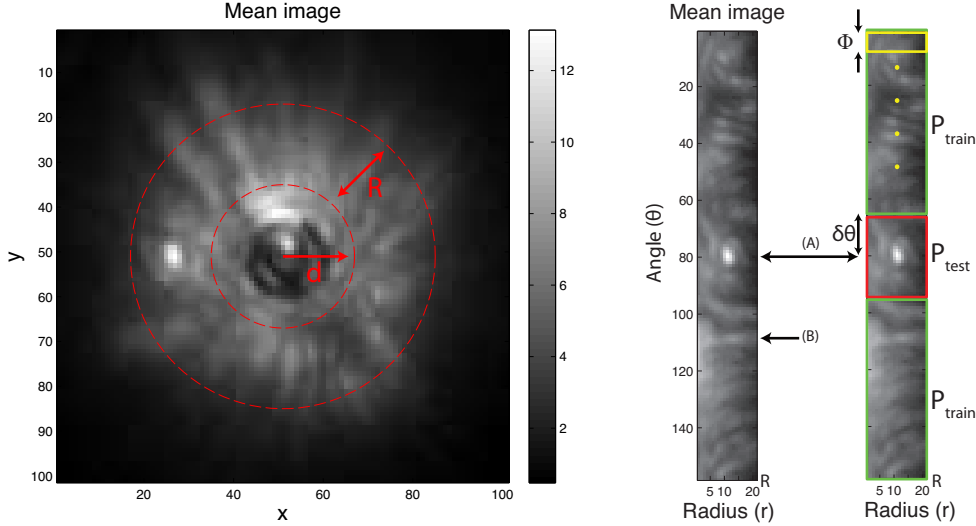


Fig. 2.— Mean over wavelength Λ and cubes N for the star FU Ori. *Left*: Cartesian representation, with a typical annular region highlighted. Note the presence of a companion at the 9 o'clock position. *Middle*: Polar representation J of the annular region. *Right*: The PCA model is applied to overlapping patches (yellow) of angular width Φ extracted from J (also having extent Λ over wavelength). We test for a companion at a given angle, for example, (A) by first training a PCA model on patches P_{train} taken outside a zone (of half-width $\delta\theta$) around angle (A). The model is then used to reconstruct test patches P_{test} near (A).

$\forall (n, \theta \pm \delta\theta)$, where $\delta\theta = 5 - 10$ pixels typically. The training set P_{train} is the union of patches from all other angles, as illustrated in Fig. 2(right).

To build the PCA model, we reformat the training set of patches into a 2D data matrix of size $n_{samples} = ((\Theta - 2\delta\theta - 1) \cdot N)$ samples by $n_{dims} = (R \cdot \Phi \cdot \Lambda)$ dimensions. We then center the data (subtract off the mean over all samples) and build the covariance matrix (of size $n_{samples} \times n_{samples}$). We then compute the eigenvectors of the covariance matrix using singular value decomposition (SVD), which returns an eigenvalue-ranked list of eigenvectors. Each eigenvector can be reformatted back into a $[R \times \Phi \times \Lambda]$ synthetic patch, as shown in Fig. 4(left). Fig. 4(right) shows the sorted eigenvalues, revealing that most of the variance is captured with 50 or so components. Using this representation, the model for the patches is arbitrary linear combinations of the first K eigenvectors, where K is a control parameter that dictates the freedom of the model.

Given the K top eigenvectors from the training set, each patch in the test set can be reconstructed by finding the linear combination that minimizes the total squared reconstruction

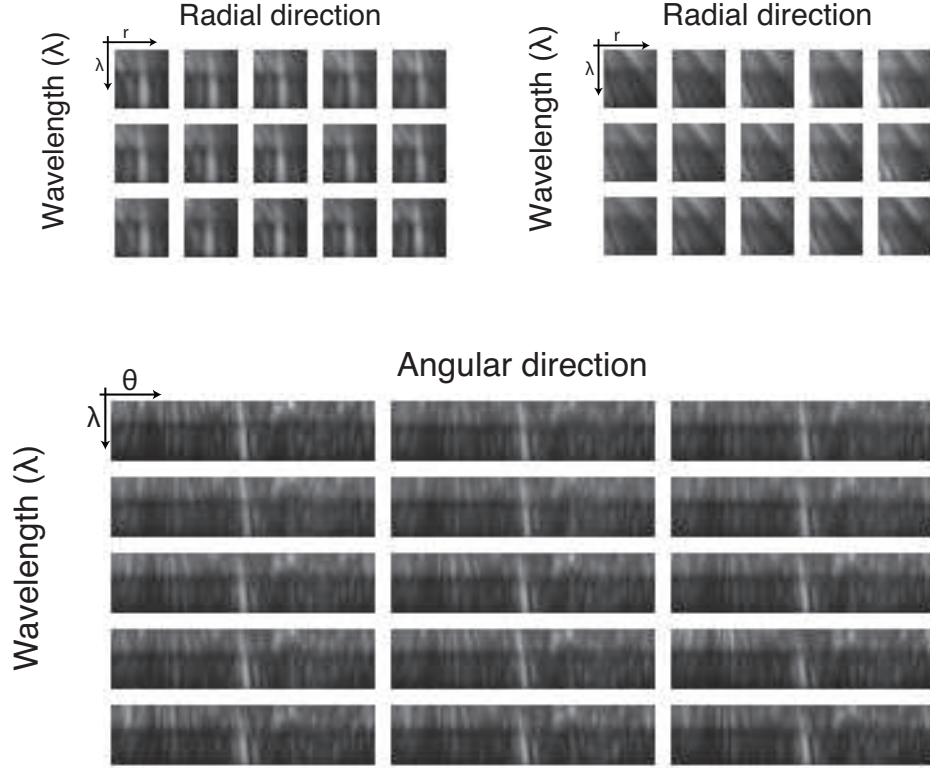


Fig. 3.— Different visualizations of the polar data volume $J_{r,\theta,\lambda,n}$ for the star FU Ori, with $N = 15$ cubes. *Top*: Each tile is of dimension $\Lambda \times R$ and shows the radial evolution of the speckles in each cube, for two fixed angles (left and right), where the companion is and is not present, respectively. The angles are indicated by (A) and (B) in Fig. 2(right). The diagonal structure of the speckles contrasts with the vertical structure of the companion (whose radius is constant with wavelength). In practice the patches P used in our model have extent 3 in the angle dimension, rather than 1 as shown in these tiles. *Bottom*: Each tile is now $\Lambda \times \Theta$, for a constant radial location. Note that the angle of the speckles is mostly constant as a function of wavelength, i.e. they move radially within the cubes. This justifies our use of patches which are small in the θ dimension.

error (residual). The optimal patch reconstruction $\hat{p}^{d,\theta,n}$ is given by $(VV^T(p^{d,\theta,n} - \mu^{d,\theta})) + \mu^{d,\theta}$, where V is a matrix of eigenvectors (of size $[(R \cdot \Phi \cdot \Lambda) \times K]$), $\mu^{d,\theta}$ is the mean over all training patches and $p^{d,\theta,n}$ is a vectorized test patch. Reshaping the reconstruction back into a $[R \times \Phi \times \Lambda]$ patch, we compute the residual error $\Delta P^{d,\theta,n} = (\hat{P}^{d,\theta,n} - P^{d,\theta,n})$.

If there happens to be a companion centered at location (d, θ, n) and if the model is not

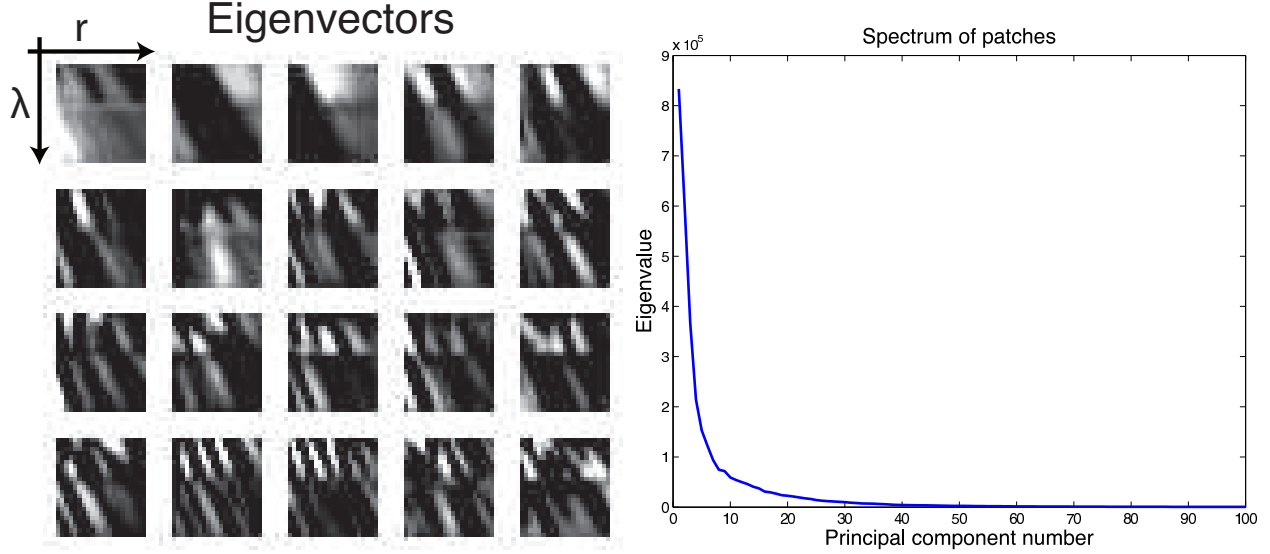


Fig. 4.— *Left*: The top $K = 20$ eigenvectors, each reshaped to be $\Lambda \times R$ (after taking the middle ϕ slice to ease visualization). *Right*: Associated eigenvalue spectrum of the data. Note that 50 or so eigenvectors are sufficient to capture most of the energy of the signal, showing that the speckle pattern, while complex, is inherently low-dimensional in the polar patch space.

so free (for at least some values of K) that it can fully absorb it, then the residual $\Delta P^{d,\theta,n}$ ought to look something like a companion, since the vertical structure of the companion cannot be modeled well by eigenvectors that consist of mainly diagonal structure. If there is no companion, then the residual should be small in magnitude and have little structure. These two scenarios are illustrated in Fig. 5.

The rationale behind splitting the data into separate train and test sets is that if the same data was used for both roles, then the model would easily over-fit the data, leaving minimal residual even if a companion was present. Holding out patches around the test location when building the PCA basis ensures that the test data is unseen, thus the model is forced to generalize from the training data when reconstructing the test patches, rather than memorizing its peculiarities. The importance of this hold-out procedure is demonstrated in Fig. 6. However, as we exhaustively search all d, θ locations, the training and test sets are different for each and thus the PCA basis must be recomputed each time. In practice, this is the computational bottleneck of the scheme, since SVD takes some seconds to compute the eigenvectors given that $n_{dim} \sim 2000 - 3000$.

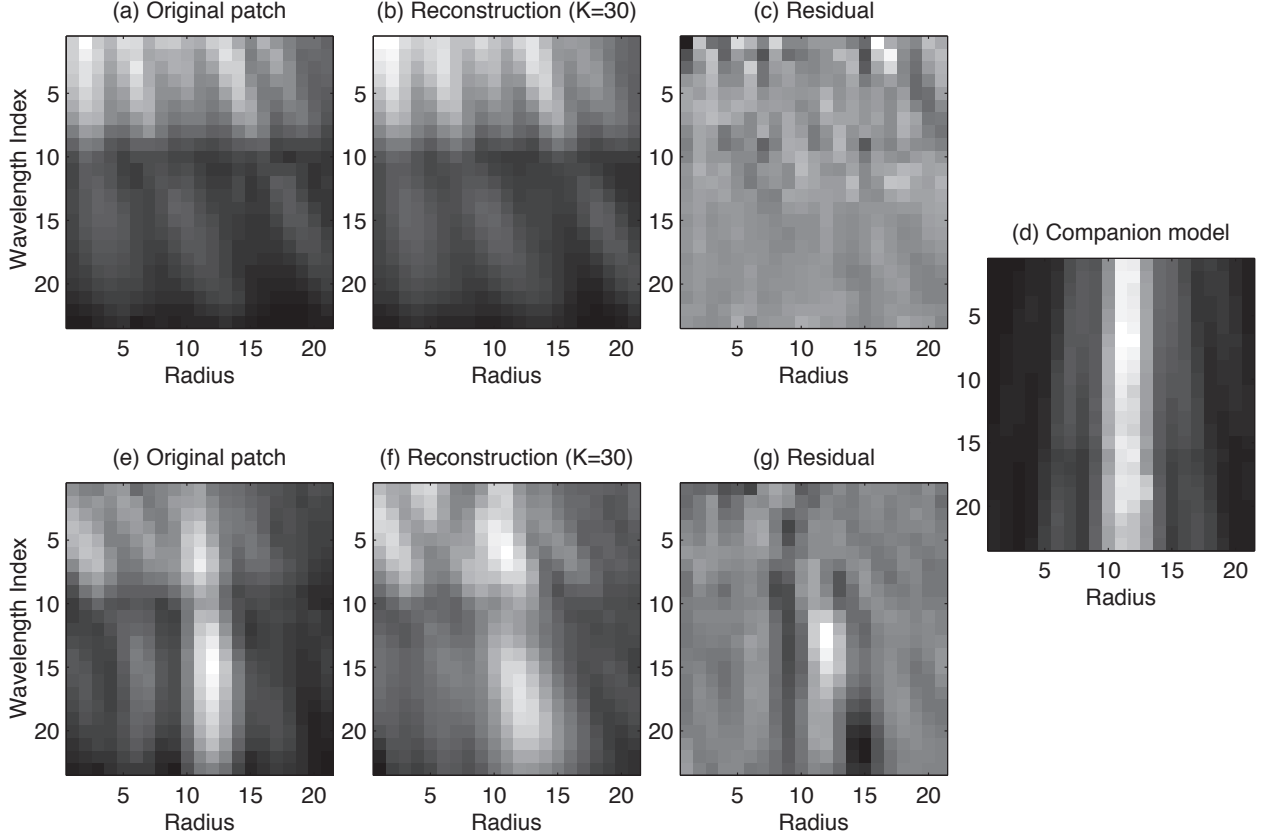


Fig. 5.— Reconstructions using our PCA model with $K = 30$ components (averaged over angle ϕ). (a): Typical patch, containing only speckles. (b): Reconstruction using our PCA model with $K = 30$. (c): Error residual. Note the lack of structure. (d): Companion model, which has low correlation with (c). Note the Airy rings around the core, that spread out with wavelength. (e): Patch containing companion. (f): Reconstruction from our model. (g): The error residual shows clear structure associate with the companion, i.e. the PCA speckle model cannot reconstruct well the companion signal. This has high correlation with the companion model of (d).

2.4. Correlation with Companion Model

As illustrated in Fig. 5, the PCA model should leave some structure of the companion (if present) in the residual signal. We therefore cross-correlate the residual patches $\Delta P^{d,\theta,n}$ with a *companion model* C . This is a patch of dimension $[R \times \Phi \times \Lambda]$ containing a centered point-spread function, obtained by polar transforming the cartesian calibration data (using the appropriate Jacobian). Since the spectrum of the companion is not known ahead of time, a “white spectrum” is used for the companion model, i.e. uniform intensity at each wavelength band. The companion model is shown in Fig. 5(d).

The amplitude of the cross-correlation signal is averaged over cubes n to give a detection signal at location d, θ . In practice, we find that normalizing the residual patches to have unit ℓ_2 length performs better since it avoids a bias towards smaller values of d where the residuals tend to be larger. The normalized detection response $o(d, \theta)$ is computed as:

$$o(d, \theta) = \sum_{n=1}^N \frac{\left(\sum_{r=1}^R \sum_{\phi=1}^{\Phi} \sum_{\lambda=1}^{\Lambda} \Delta P_{r,\phi,\lambda}^{d,\theta,n} \cdot C_{r,\phi,\lambda} \right)}{\|\Delta P_{r,\phi,\lambda}^{d,\theta,n}\|_2} \quad (1)$$

Fig. 6 shows the detection response $o(d, \theta)$ and residual error magnitude for the example region shown in Fig. 2. When computing $o(d, \theta)$, it is also possible to average over the Φ patches that overlap with a given angle θ . However, we found that this tended to blur out the detection signal.

Finally, the detection response $o(d, \theta)$ exists in the polar domain and we transform it back the cartesian domain to produce a final detection map $m(x, y)$.

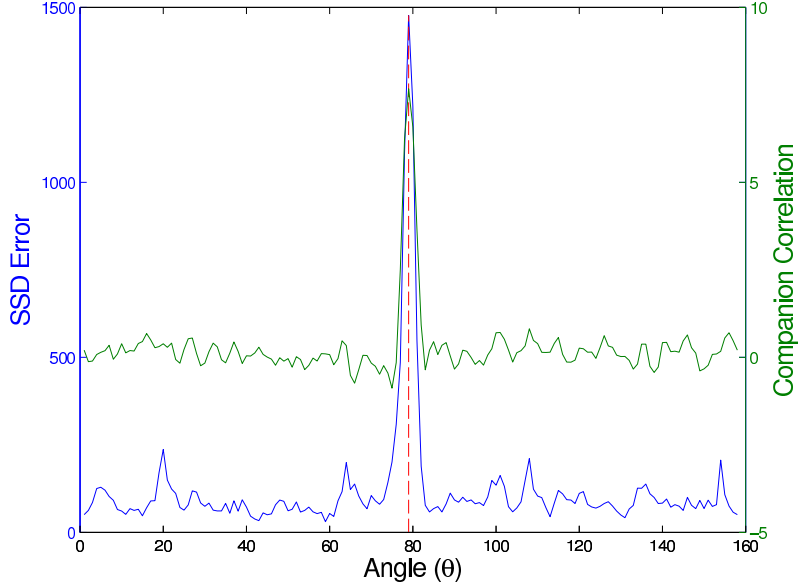


Fig. 6.— A detection signal (green) $o(d, \theta)$ for the example annular region shown in Fig. 2 at radius d . The sum of the squared residual error is shown in blue. Both curves have a distinct peak at the angle corresponding to the location of the companion (red).

2.5. Implementation

Pseudo-code for the algorithm is given in Algorithm 1. A Matlab implementation of the algorithm is provided on the project webpage: <https://p1640.amnh.org/p1640/software/S4/>,

Algorithm 1 The S_4 Algorithm

Require: Data volume I of dimension $[X \times Y \times \Lambda \times N]$, Companion model C

Require: # Components K

Require: Patch width Φ , Ring width R , Test region half-width $\delta\theta$

```
1: Spatially center  $I$ 
2: for  $d = 1$  to  $(X/2 - R)$  do %% Loop over radius
3:    $J$  = Polar transform of annular region of  $I$  at radius  $d$ , width  $R$ 
4:    $P$  = Patchify  $J$  using patches of angular width  $\Phi$ 
5:   for  $\theta = 1$  to  $\Theta$  do %% Loop over angle
6:      $P_{test} = P$  in region  $\pm\delta\theta$  around  $\theta$ 
7:      $P_{train} =$  all  $P$  not in  $P_{test}$ 
8:     Compute largest  $K$  eigenvectors  $V$  and mean  $\mu$  from  $P_{train}$ 
9:      $\hat{P}_{test}$  = reconstruction of  $P_{test}$  using  $V$  and  $\mu$ 
10:    Compute residual  $\Delta P = \hat{P}_{test}(\theta) - P_{test}(\theta)$ 
11:    Normalize  $\Delta P$  to unit length
12:     $o(d, \theta)$  = correlation of  $\Delta P$  with companion model  $C$  (Eqn. 1)
13:     $m(x, y)$  = inverse polar transform of  $o(d, \theta)$ 
14:  end for
15: end for
16: Output: Detection map  $m$ 
```

with accompanying instructions and examples. Beyond the core Matlab package, it also requires the Image Processing toolbox and runs on Windows, Mac and Linux platforms. The code is also compatible with Octave, an open-source version of Matlab. The run-time of the algorithm is around 8 hours for a given star using typical settings, on a fast PC and has a modest memory requirement (a few Gb).

3. Results on Synthetic Data

We initially demonstrate our approach using companions inserted into real several stars recorded from the P1640 instrument: Alcor, HD87696 and GJ758. The input to our algorithm consists of data cubes from the extraction and spectral calibration pipeline, numbering 5, 10 and 15 for the three stars, respectively.

Our evaluation consists of inserting fake companions of varying intensity into data cubes and measuring the statistical significance of peak at the true location. GJ758 and HD87696

have no detectable genuine sources¹ that might confuse the evaluation. Alcor does have a companion (Alcor B) but it is sufficiently far from the star that it has been cropped from the data cubes we use for testing our algorithm. We use a fake companion that has a very similar spatial structure to the companion model C , but differs in spectrum: the fake has a realistic reddish spectrum while model C is white.

We quantify the strength of the inserted source by measuring its mean brightness over a 5 by 5 spatial window *relative* to the mean speckle brightness in 5 by 5 window at a given location, averaging over wavelength and cube. Put another way, under this measure a 5% inserted companion at two different locations has different absolute brightness, but the same companion/speckle brightness ratio.

We characterize the statistical significance of the detected peak in two ways. First, we measure how many standard deviations it is above the rest of the detection map. The background of the detection map has statistics that are close to Gaussian, making this a valid comparison. Second, we show the rank of the peak, relative to all other elements in the map. A rank of 1 indicates that it is the strongest peak in the entire map. This test does not make any assumptions about Gaussianity of the data and is similar in spirit to other non-parametric tests such as the Wilcoxon-rank sum test.

All experiments used the following settings: $R = 30$ pixels, $\delta\theta = 10$ pixels and $\Phi = 3$ pixels. Performance is relatively insensitive to the first two of these. $\Phi = 3$ is superior to $\Phi = 1$ and similar to $\Phi = 5$. But $\Phi = 5$ is not preferred as it significantly increases the dimensionality of the PCA space, which slows the algorithm considerably.

The number of components in the PCA model, K , is an important parameter in the algorithm and for each experiment we vary this systematically and show detection maps m for the best performing value, which is typically around $K = 100$. If K is too small, the PCA model will not be able to reconstruct the speckles well. If K is too large it will also reconstruct the companion, leaving nothing in the residual. See Fig. 7 for an illustration of this. Fig. 7 also demonstrates how the fake sources are inserted and what the PCA residuals look like, before correlation with the companion model.

Fig. 8 shows the fake sources added to $N = 5$ cubes of star HD87696. Both the location and brightness of the source are varied, the latter from 1–4% of the speckle brightness at the insertion location, thus being a relative, not absolute, measure of detection performance. Table 1 presents these results in a different form, showing the number of standard deviations

¹GJ758 has a stellar companion (see Janson et al. (2010)), but this is outside the field-of-view for our data.

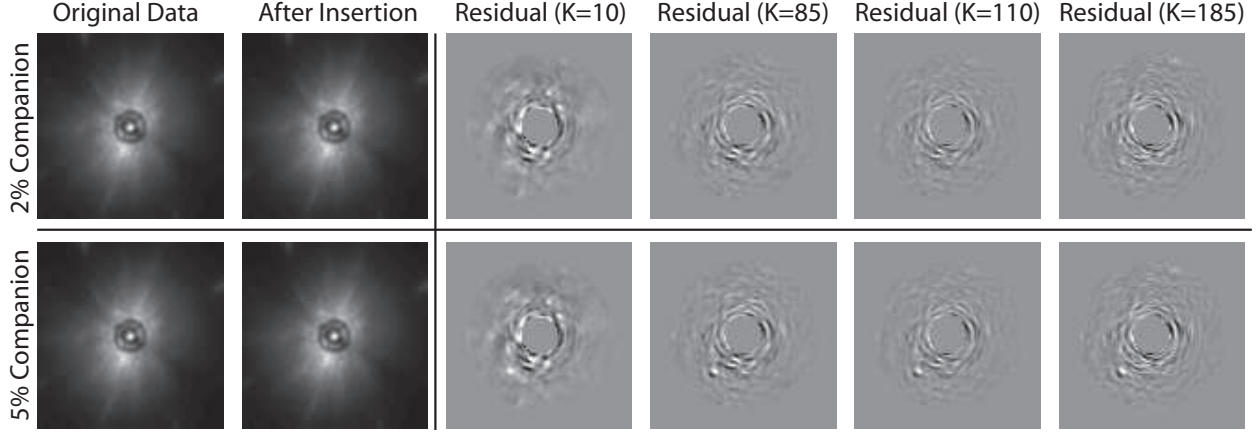


Fig. 7.— A single cube of HD87696 (averaged over wavelength), along with PCA residuals for fake companions of 2% and 5% relative intensity (top and bottom rows, respectively), inserted at the 7 o’clock position. Columns from L to R: (i) Original cube. (ii) Cube after insertion of fake companion. (iii)-(vii): PCA residuals ΔP mapped back to a cartesian representation for $K = \{10, 85, 110, 185\}$. The dynamic range used in plotting decreases across the row (but is constant within a column), since increasing K reduces the residual magnitude. Note: (a) invisibility of companion after insertion (compare columns (i) & (ii)). (b) 5% insertion is visible in residuals, while 2% is not. Correlating these residuals with a companion model makes detection below 2% possible (see Fig. 8 and Fig. 9). (c) Too few components ($K = 10$) or too many ($K = 185$) reduce the contrast of the companion relative to speckle residuals, thus impairing detection performance.

above the background, as well as the rank of the true companion location versus other local maxima in the response map. Taking a 3σ threshold, we see that the algorithm can reliably detect the companion down to around 1-2% of the speckle brightness.

By assuming that no genuine companions are present in the detection maps m , any strong peaks in the detection signal must be due to noise. This allows us to compute a sensitivity map which records at each location the brightness level of a companion whose detection signal in m just exceeds the largest magnitude noise peak. Fig. 9 shows sensitivity maps for three different stars, HD87696, Alcor and GJ758. The maps show the sensitivity is mostly at the the 1-2% level, consistent with the other results. In areas near the occulting disk, however, the sensitivity is poor (worse than 10%). The performance of the algorithm is highly dependent on the quality of the input data, which varied between the stars.

The sensitivity maps in Fig. 9, allow us to derive a measurement of absolute contrast. At a given location this is done by combining the sensitivity (i.e. minimum detectable companion brightness, relative to the background speckles) with the ratio of the speckle brightness to the

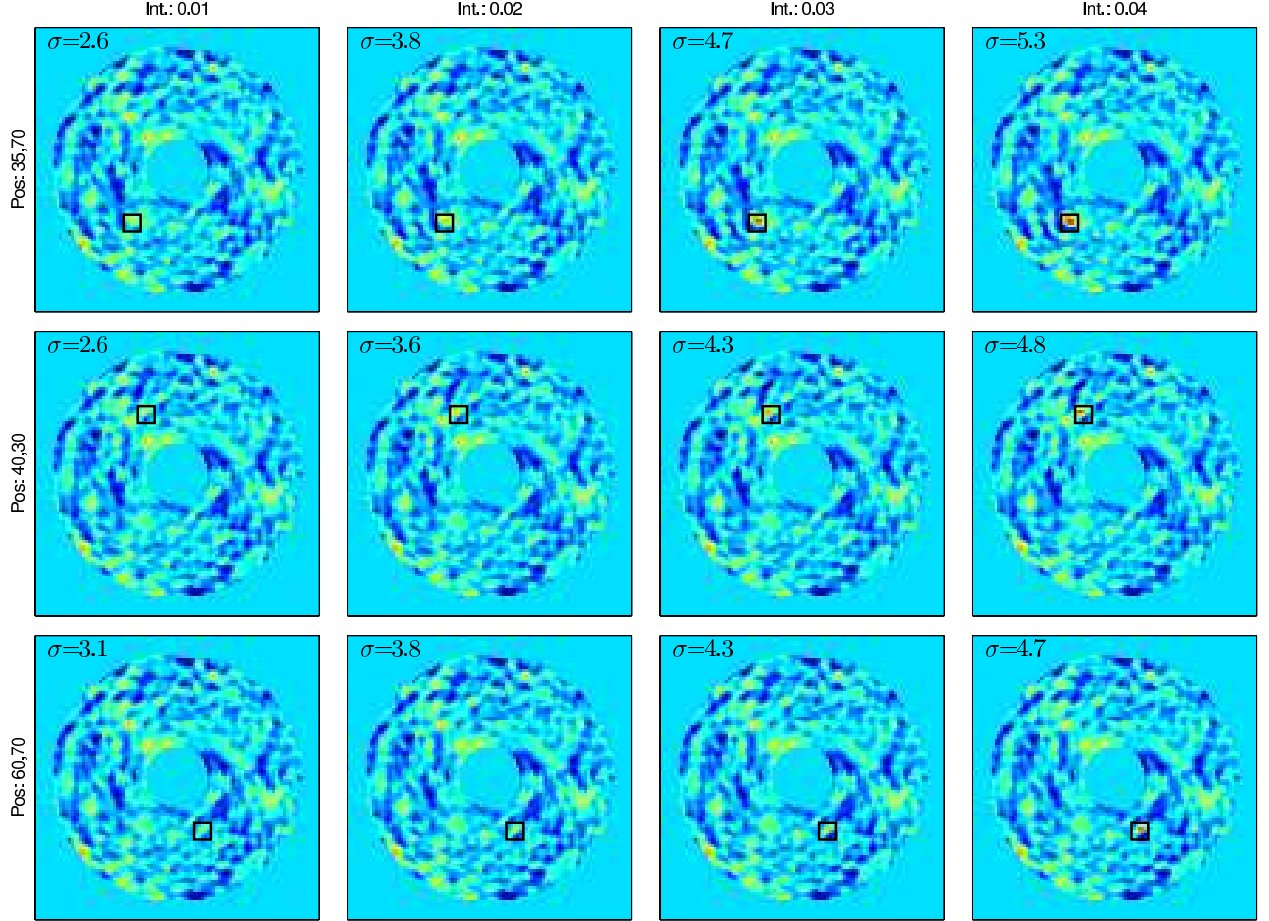


Fig. 8.— Cartesian detection output maps m for the star HD87696, for fake companions inserted at 3 different locations at 1,2,3 and 4% relative intensities. Red and yellow corresponds to a high response, blue corresponds to a low response. The cyan areas are not examined due to boundary issues caused by the width of the annular section. The black rectangle shows the true location of the inserted source. Each plot gives the statistical significance of the detection. The algorithm is able to reliably detect the companion down to between 1-2% of the speckle flux. The figure is best viewed in electronic form.

unocculted star. Averaging over each annulus gives the plots shown in Fig. 10, which show the absolute contrast as a function of radius and wavelength before and after the application of the S4 algorithm to the P1640 data from HD87696 and GJ758. S4 can be seen to give an improvement in detection sensitivity of around 2 orders of magnitude, reaching 10^{6-7} contrast for outer radii. Furthermore, S4 compensates for the chromatic behavior of the coronagraph, as shown by the softening of the contrast's dependence on wavelength.

Shot-noise due to photon arrival times and the total exposure time provides a physical

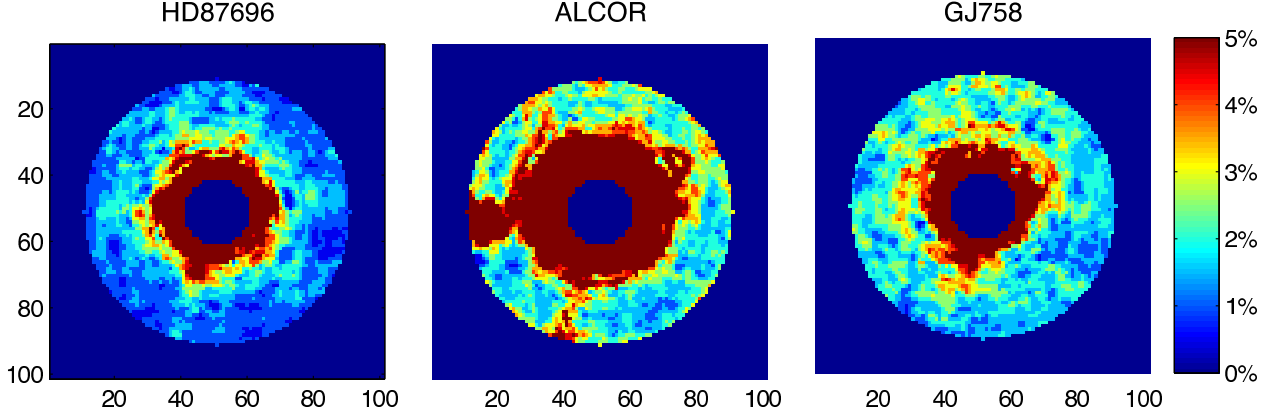


Fig. 9.— Cartesian detection sensitivity maps for stars HD87696, Alcor and GJ758. The color shows the detection threshold at each location, as a fraction of the speckle flux at that location. Red corresponds to a high response, blue corresponds to a low response. Dark blue regions are those non-examinable due to the width R of the annular region. The performance of the algorithm depends on the quality of the cubes input to the algorithm, which was noticeably worse for Alcor than the other two stars. In the case of HD87696, which has the best quality cubes, large portions of the map are around (or below) 1%.

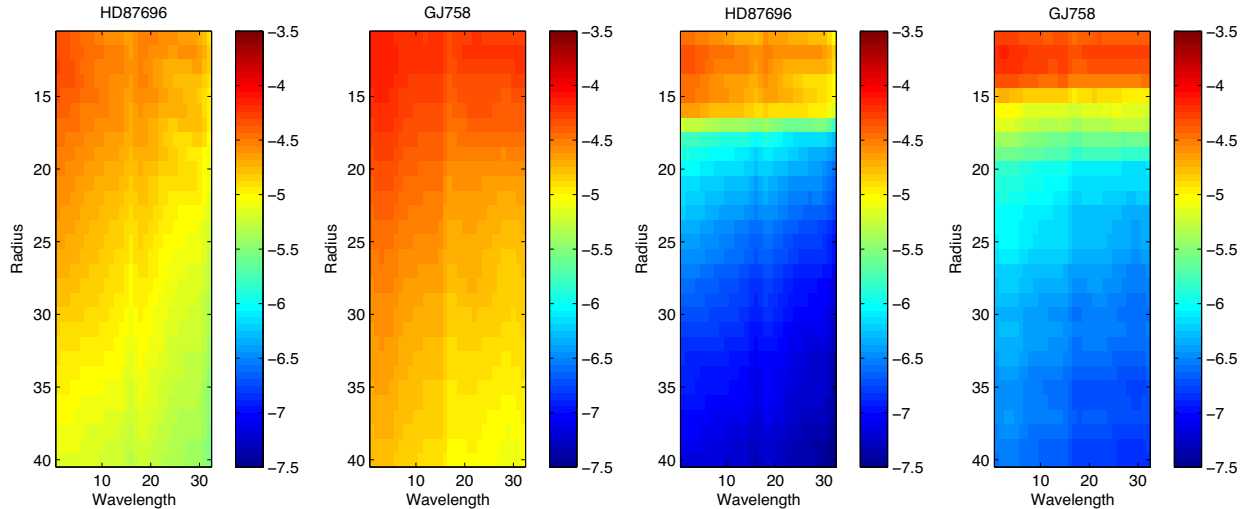


Fig. 10.— Absolute contrast as a function of radius and wavelength before (L) and after (R) the application of S4 to two stars, HD87696 and GJ758. Shown in \log_{10} scale. S4 give around 2 orders of magnitude improvement, reaching 10^{6-7} absolute contrast for outer radii.

lower-limit to companion detection. We compute the absolute 2D shot noise map $s(x, y)$ as:

$$s = \sqrt{T \cdot (\tilde{C} * \frac{1}{N} \sum_n \sum_{\lambda} I_{x,y,\lambda,n})} \quad (2)$$

where T is the exposure time (secs), $*$ is a 2D correlation operation and \tilde{S} is a 2D binary mask of the companion model, where all but the brightest central core of the wavelength-averaged companion model C has been thresholded to zero. The correlation has the effect of summing over all pixels used in the companion model (the companion occupies more than a single pixel). In Fig. 11, we plot the ratio of s to the data I , to give the same relative measure used when producing the sensitivity maps shown in Fig. 9. In the case of HD87696, we see that the shot-noise limit is $\sim 0.4\%$ around the periphery and $0.25 – 0.3\%$ near the star. Our algorithm’s sensitivity map of HD87696 has large regions within a factor of 4 of the shot-noise limit. However, close in to the star, the our sensitivity drops to $> 5\%$, considerably worse than the limit.

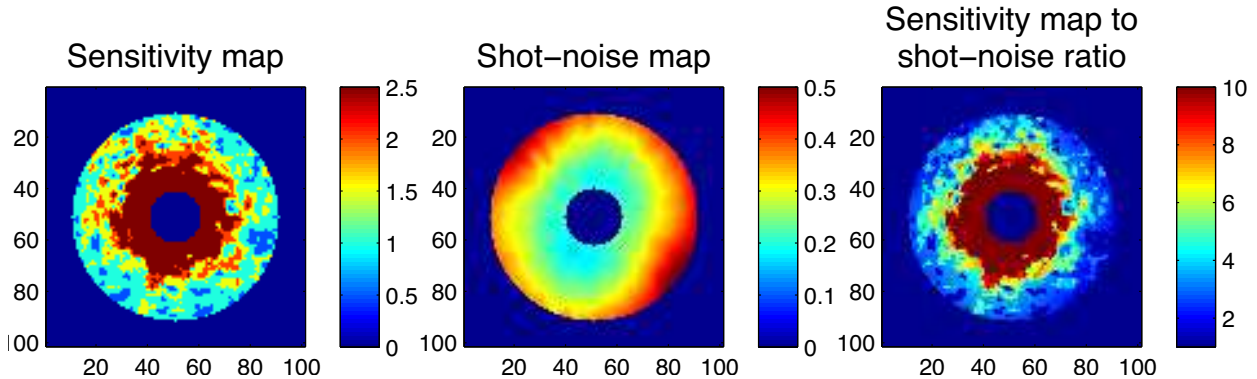


Fig. 11.— The detection capability of our algorithm, compared to the physical limit imposed by shot-noise in the detector, for star HD87696. *Left:* Detection sensitivity map (same as Fig. 9(left), but different dynamic range). Units are % relative to the speckle intensity. *Middle:* Shot noise map, computed using Eqn. 2. Units are % relative to the speckle intensity. *Right:* Ratio of the sensitivity map to the shot-noise limit. In places, our algorithm is close to the shot-noise limit (i.e ratio < 2), but typically it is within a factor of 4, apart from regions close to the star.

3.1. Comparison to LOCI

We also perform a direct comparison to the damped LOCI algorithm Pueyo et al. (2011), an improved variant of the original algorithm (Lafreniere et al. (2007)). Data cubes with fake companion insertions at five randomly chosen locations were created and provided to the authors of Pueyo et al. (2011). They ran their damped LOCI implementation on the data cubes and returned the results, enabling their evaluation under the metrics used above. The cubes were also presented to our algorithm, using the settings described above. Thus, both the input data and the evaluation metrics were the same, the only difference being

the detection algorithm itself. Table 2 shows compares the companion rank of the two algorithms for different brightnesses of fake companion. At the 2% level, S_4 has significance values $\geq 3.9\sigma$ for all five companion locations, where are LOCI drops to 1.8σ for some positions. At the 1% level, neither algorithm reliably finds the true location, but S_4 has a mean significance (averaging over the 5 locations) of 2.5σ , compared to 1.8σ for LOCI. A visual comparison is shown in Fig. 12.

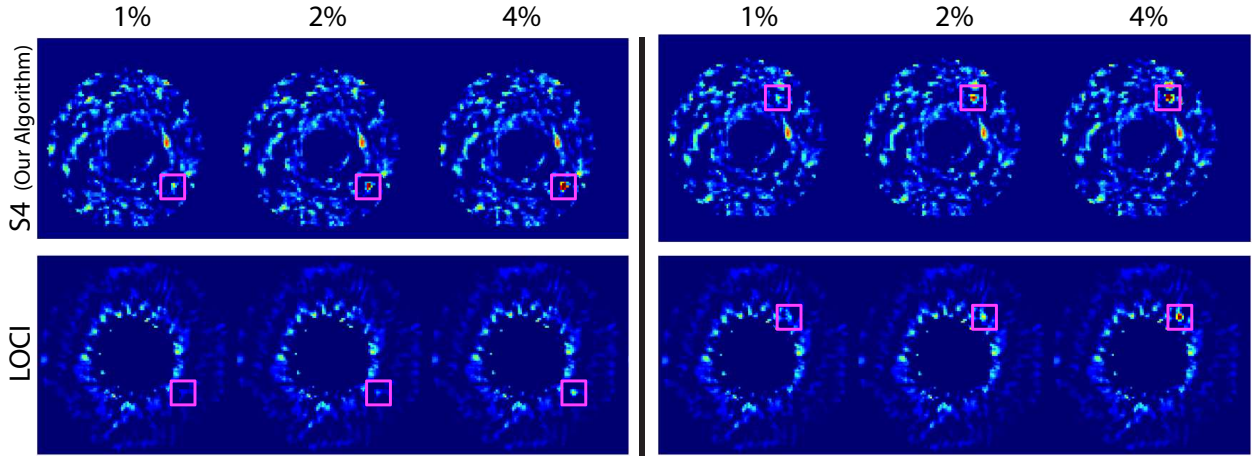


Fig. 12.— Comparison to LOCI (Pueyo et al. (2011)). Fake companion insertions (3 intensities) at two different locations. Red = higher detection level. The true location is indicated by the magenta box. Our algorithm (S_4) cleanly locates the companion at the 2% level, which is still visible at the 1% level. LOCI finds the 4% companion but the 2% one is no longer brighter than background artifacts.

4. Results on HR8799

We applied our algorithm to 10 cubes of data acquired over two consecutive nights (14/15th June 2012) of the star HR8799. Observations with the Keck telescope by Marois et al. have revealed 4 companions orbiting the star, making it an ideal test case for our algorithm.

After centering the cubes, we applied the S_4 algorithm using parameters: $R = 13$, $\Phi = 3$ and $\delta\theta = 10$. Pueyo *et al.* also applied the KLIP algorithm Soummer et al. (2012) to the same data. The results of the two algorithms are shown in Fig. 13 and Fig. 14, taken from Oppenheimer et al. (2013). The former shows the PCA residual map produced by both algorithms, with S_4 giving higher signal to noise than KLIP, enabling the clear detection of the (d) companion. Applying the companion model to the residual produces the output map

shown in Fig. 14. This gives cleaner detections, with three of the peak above 3σ significance. Oppenheimer et al. (2013) also used S4 to perform a spectral analysis of these companions and the algorithmic details of this study will be described in a forthcoming paper.

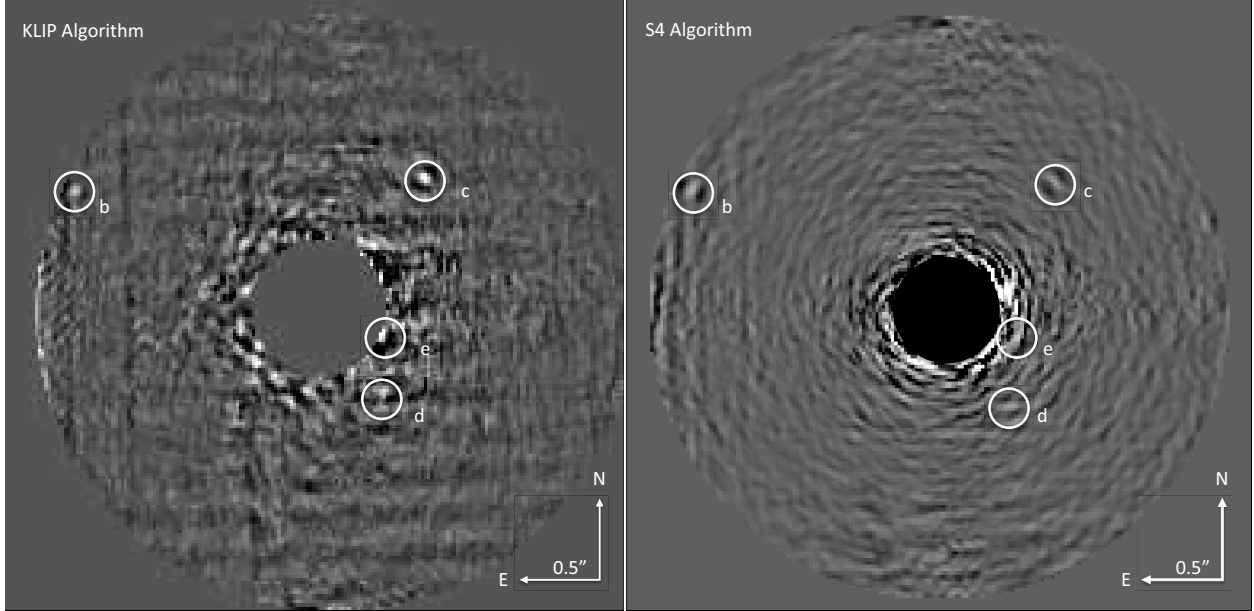


Fig. 13.— From Oppenheimer et al. (2013): HR8799 PCA residual maps for the *KLIP* algorithm Soummer et al. (2012) (L) and S4 (R). While (b) and (c) companions are clearly visible in both maps, the (d) companion is clearer in S4. The (e) companions are weak in both. Note that for S4, this residual map is only an intermediary output. See Fig. 14 for the final output.

5. Discussion

We have introduced the *S4* algorithm for companion detection and demonstrated it on several stars captured by the *P1640* instrument. The approach outperforms the existing LOCI and KLIP algorithms by a significant margin and approaches the shot-noise limit for radii further from the star. The performance of the algorithm is dependent on the speckle structure being clearly visible within the input data. Hence, in regions close to the star which lack clear structure, the algorithm performance drops off significantly with a relative sensitivity worse than 5%. When applied to the *P1640* data, S4 improves the absolute contrast by 2 orders of magnitude, to give levels around 10^{6-7} , beyond the core region.

There are several issues with the methods presented that leave room for improvement:
 (a) We do not use a proper instrument noise model – the PCA model could be modified to

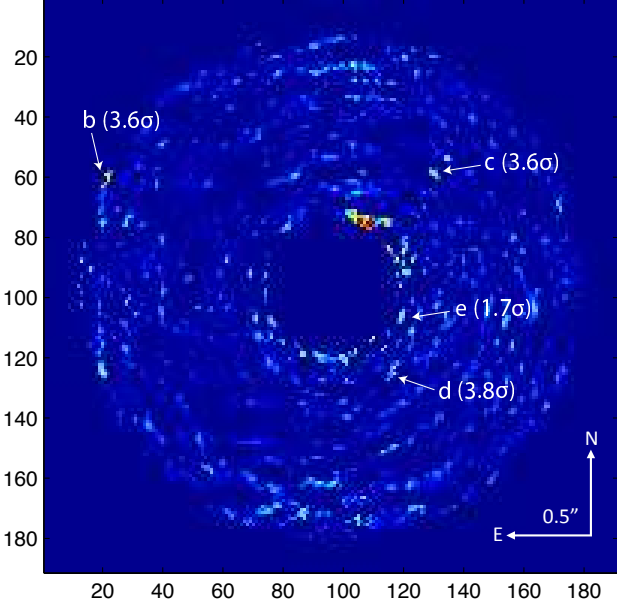


Fig. 14.— From Oppenheimer et al. (2013): The final output of S4 for HR8799. The companions have distinct peak, which for (b),(c) and (d) companions are significantly above the surrounding noise ($\geq 3.6\sigma$). Note also that the position of the companions is more precisely localized than in Fig. 13(right).

incorporate known noise properties of the instrument (such as that of Tsalmantza & Hogg (2012)). (b) Our companion model assumes a white spectral emission distribution (SED), which is clearly wrong in general. A better approach would be to let this also be unknown and fit both the speckle and companion SED simultaneously to the data. (c) We only build our model from data cubes of a single star. This severely limits the amount of training data available and necessitates the use of simple models, such as PCA. A better approach would be to draw statistical strength from observations of multiple stars captured by the *P1640* instrument. While the speckle patterns differ between stars, they undoubtedly contain similarities that can be learned. For example, given enough data, the space of likely atmospheric distortions could be learned. (d) Related to this, the model we use does not take as input any meta data about the telescope attitude (e.g. “gravitational loading” or “differential chromatic refraction”) or observing conditions in training. A more sophisticated model might leverage this information to learn dependencies on these variables. (e) If more data were available, other modeling options become viable. For example, sparse coding (Tibshirani (1996); Mairal et al. (2009)) is a more flexible model than PCA as it can capture multiple low-dimensional linear subspaces (as opposed to a single one). Another option would be discriminative approaches based on support vector machines. Replacing PCA with these approaches might deliver superior performance. (f) The input data I to our algorithm is the

result of a complex extraction pipeline whose details we have not considered in this article. It is possible that this pipeline incorporates a number of sub-optimal operations on the data that inadvertently degrade the signal-to-noise. These might be avoided if our model were to be directly applied to the raw sensor measurements.

Finally, while the algorithm has been designed for the *P1640* instrument, it can easily be applied to data from other instruments that operate on similar principles. We are working on methods for obtaining the true spectrum of the detected companions. This will be reported in a subsequent publication.

Acknowledgements

RF & DH are partially supported by NSF CDI #1124794. RF is also partially supported by a Sloan Fellowship. Project 1640 has been funded by National Science Foundation grants AST- 0520822, AST-0804417, and AST-0908484. The project also acknowledges the generous support of Hillary and Ethel Lipsitz, the Plymouth Foundation and Futdi.

REFERENCES

Amara, A., & Quanz, S. 2012, MNRAS, 427, 948

Bloemhof, E. E., Troy, M., Dekany, R. G., & Oppenheimer, B. R. 2001, ApJ, 558, 71

Crepp, J. R., Pueyo, L., Brenner, D., et al. 2011, ApJ, 729, 132

Dekany, R., Bouchez, A., Britton, M., et al. 2006, Proc. SPIE, 6272

Hinkley, S., Oppenheimer, B. R., Soummer, R., et al. 2007, ApJ, 654, 633

Hinkley, S., Oppenheimer, B. R., Zimmerman, N., et al. 2011, PASP, 123, 74

Janson, M., Carson, J., Thalmann, C., et al. 2010, ApJ, 728, 85

Lafreniere, D., Marois, C., Doyon, R., Nadeau, D., & Artigau, E. 2007, ApJ, 660, 770

Mairal, J., Bach, F., Ponce, J., & Sapiro, G. 2009, in ICML

Marois, C., Macintosh, B., & Vran, J.-P. 2010, SPIE, 7736

Oppenheimer, B. R., & Hinkley, S. 2009, ARA&A, 47, 253

Oppenheimer, B. R., Hinkley, S., Vasisht, G., et al. 2012, Proc. SPIE, 8447

Oppenheimer, B. R., Baranec, C., Beichman, C., et al. 2013, ApJ, 768

Pueyo, L., Crepp, J. R., Vasisht, G., et al. 2011, ApJS, 199, 6

Racine, R., Walker, G. A. H., Nadeau, D., Doyon, R., & Marois, C. 1999, PASP, 111, 587

Roberts, J. E., Dekany, R. G., Burruss, R., et al. 2012, Proc. SPIE, 8447

Soummer, R. 2005, ApJ, 618, 61

Soummer, R., Pueyo, L., & Larkin, J. 2012, ApJ, 755

Tibshirani, R. 1996, Journal of the Royal Statistical Society, 58

Traub, W. A., & Oppenheimer, B. R. 2010, in Exoplanets, ed. S. S. (University of Arizona Press)

Tsalmantza, P., & Hogg, D. W. 2012, ApJ, 753

Wallace, J. K., Burruss, R. S., Bartos, R. D., et al. 2010, Proc. SPIE, 7736

Zhai, C., Vasisht, G., Shao, M., et al. 2012, Proc. SPIE, 8447

Zimmerman, N., Brenner, D., Oppenheimer, B. R., et al. 2011, PASP, 123, 746

Zimmerman, N., Oppenheimer, B. R., Hinkley, S., et al. 2010, ApJ, 709, 733

Location	X	Y	0.5%	1%	2%	3%	4 %	5%	7.5%	10%
1	35	70	0.7 / 32	1.9/ 19	3.9/ 1	5.4/ 1	6.6/ 1	7.4/1	8.7/1	9.3/ 1
2	40	30	2.1/7	2.8/ 7	4.1/ 1	5.2/ 1	6.1/ 1	6.9/ 1	8.3/ 1	9.2/ 1
3	60	70	-	2.7/ 6	4.4/ 1	5.7/ 1	6.8/ 1	7.6/ 1	8.7/1	9.1/ 1
4	65	35	1.2/28	1.9/22	3.1/ 3	4.1/ 1	5.0/ 1	5.7/1	6.8/ 1	7.4/ 1

Table 1: Synthetic companion insertion on HD87696. For 4 different locations and fake source intensities ranging from 0.5% to 10%, relative to the local speckle level. For each combination, we give the number of standard deviations above the background, as well as the rank of the peak over the entire map. A rank of 1 means that the strongest local maxima in the detection map is at the true location of the inserted source (i.e. it has correctly found the companion). Rank n means that the local maxima containing the companion is the n strongest in the detection map. Our algorithm is reliable (i.e. $\geq 3\sigma$) for companion brighter than 2% of the speckle flux.

Location	X	Y	Method	1%	2%	4%	6%
1	26	72	S_4 :	2.9 / 3	5.2 / 1	7.2 / 1	7.8 / 1
			LOCI:	1.8 / 31	3.0 / 10	5.7 / 1	8.3/ 1
2	30	40	S_4 :	4.2 / 2	5.5 / 1	6.9 / 1	7.4 / 1
			LOCI:	3.1 / 2	4.6 / 1	7.4/ 1	10.1 / 1
3	56	72	S_4 :	2.2 / 3	3.9 / 1	6.0/ 1	7.0/ 1
			LOCI:	0.8 / 7	-	7.5/ 1	-
4	67	30	S_4 :	2.3 / 6	4.5/ 1	7.0 / 1	8.0 / 1
			LOCI:	2.2/ 23	3.8 / 3	6.9/ 1	-
5	75	70	S_4 :	1.1/ 5	4.1/ 1	7.9 / 1	8.5/ 1
			LOCI:	1.1 / 56	1.8 / 31	3.5 /16	5.1/ 1

Table 2: A comparison between damped LOCI (Pueyo et al. (2011)) and our algorithm (S_4) for five different locations on star HD87696. We give the number of standard deviations above the background (1st number) and rank (2nd number) of the true peak. S_4 typically has higher significance values (and lower rank) than LOCI.